

# Progress Toward the First Search for Bound Neutron Oscillation into Antineutron in a Liquid Argon TPC

MICROBOONE-NOTE-1093-PUB

The MicroBooNE Collaboration

August 3, 2020

## Abstract

This note presents current progress for a neutron-antineutron oscillation ( $n - \bar{n}$ ) search in MicroBooNE paving the way for the first search analysis of such process in a Liquid Argon Time Projection Chamber (LArTPC). Convolutional Neural Network (CNN) and Boosted Decision Tree (BDT) algorithms were used to select signal  $n - \bar{n}$  events over cosmogenic backgrounds. The CNN-only, BDT-only, and the combined (CNN+BDT) methods were demonstrated on the Monte-Carlo signal and background events. Validation of the CNN-only and the BDT-only methods was carried out on a small dataset of MicroBooNE Run1 off-beam data, setting the starting point toward further improvement of the analysis.

# Contents

<b>1</b>	<b>Introduction</b>	<b>3</b>
<b>2</b>	<b>Analysis Overview</b>	<b>4</b>
<b>3</b>	<b>Preliminary Results</b>	<b>6</b>
3.1	CNN-only analysis . . . . .	6
3.2	BDT-only analysis . . . . .	7
3.3	Combined analysis . . . . .	9
<b>4</b>	<b>Conclusions</b>	<b>13</b>

# 1 Introduction

Neutron-antineutron oscillation is a baryon number (B) violating process ( $\Delta B = 2$ ) predicted by theories beyond the Standard Model [1, 2]. This process can be searched for, experimentally, with free neutron beams (see, e.g. [3]) or with nucleus-bound neutrons in large, underground detectors well-shielded from backgrounds.

In nucleus-bound neutron oscillation, a neutron inside a parent nucleus spontaneously transitions (“oscillates”) into an antineutron, with a probability determined by the mean vacuum (free)  $n - \bar{n}$  transformation period as well as a nucleus-dependent nuclear suppression factor, given that the oscillation takes place within a strong potential. For argon, nuclear suppression factors have been theoretically estimated to be  $T_R^{Ar} = 5.6 \times 10^{22} s^{-1}$  [4].

Following this oscillation, the resulting antineutron annihilates with a neighboring nucleon; free nucleon-antineutron annihilation at rest is expected to result in, typically, 3-5 final state pions, with a net momentum of zero and a total energy corresponding to the sum of the two nucleon masses. The branching ratios of this annihilation process are shown in Tab. 1. In the case of bound neutron oscillation searches, because this process is expected to take place inside a nucleus, initial and final state nuclear effects such as Fermi motion of the original neutron, and hardonic interactions of final state pions as they exit the nucleus, come into effect, and distort this predicted annihilation signature. Such effects can be modeled using a number of generators; for the analysis presented in this note, the GENIE event generator [5] v3.0.2 is used to fully simulate this process, including nuclear effects.

$(\bar{n}, p)$		$(\bar{n}, n)$	
channel	branching ratio	channel	branching ratio
$\pi^+ \pi^0$	1%	$\pi^+ \pi^-$	2%
$\pi^+ 2\pi^0$	8%	$2\pi^0$	1.5%
$\pi^+ 3\pi^0$	10%	$\pi^+ \pi^- \pi^0$	6.5%
$2\pi^+ \pi^- \pi^0$	22%	$\pi^+ \pi^- 2\pi^0$	11%
$2\pi^+ \pi^- 2\pi^0$	36%	$\pi^+ \pi^- 3\pi^0$	28%
$2\pi^+ \pi^- 2\omega$	16%	$2\pi^+ 2\pi^-$	7%
$3\pi^+ 2\pi^- \pi^0$	7%	$2\pi^+ 2\pi^- \pi^0$	24%
		$2\pi^+ 2\pi^- \omega^0$	10%
		$2\pi^+ 2\pi^- 2\pi^0$	10%

**Table 1:** Effective branching ratios of  $(\bar{n}, p)$  and  $(\bar{n}, n)$  annihilation for argon, excerpted from Table 5.3 of [6].

The future Deep Underground Neutrino Experiment (DUNE) is projected to be able to search for argon-bound neutron oscillations into antineutrons with sensitivity which represents a factor of 1.5 improvement [7] relative to the current best limits to bound neutron oscillations, from Super-Kamiokande [8]. The DUNE analysis in [7] uses machine learning techniques, in particular image analysis of event-level information, using Convolutional Neural Networks (CNNs), trained and tested with simulations. Image analysis techniques especially involving deep learning have generally shown great promise and excellent performance in applications to liquid argon time projection chamber (LArTPC) data analysis. For example, MicroBooNE has demonstrated successful neutrino interaction identification and final state particle classification [9] and pixel-type identification [10] using such techniques.

The analysis presented in this note seeks to demonstrate that event-level identification using image analysis is a viable application for rare event searches in LArTPC’s, and furthermore aims to provide the first ever search for argon-bound neutron-antineutron oscillation in a LArTPC, using MicroBooNE data. Even though the MicroBooNE detector size is too small to provide

competitive limits, and overwhelmed with cosmogenic activity as it is operating on-surface rather than deep underground, it will serve as a valuable first step toward realizing DUNE’s future search with significantly higher sensitivity.

In the following section, we describe the neutron-antineutron oscillation search analysis followed by MicroBooNE, adapted from [7]. Next, we present preliminary results; specifically, we show data-to-Monte Carlo comparisons with a small sample of unblinded data from MicroBooNE’s Run 1. Finally, we provide, as an example, MicroBooNE’s projected sensitivity with the full Run 1 data set, using unoptimized final selection cuts.

## 2 Analysis Overview

Both the DUNE and MicroBooNE neutron-antineutron oscillation searches use traditional reconstruction and image-based analysis to select events consistent with a neutron-antineutron oscillation signature, and to isolate them from cosmogenic or atmospheric neutrino backgrounds. Traditional reconstruction makes use of the Pandora reconstruction framework for LArTPCs [11] and BDT-based selection, while image-based analysis makes use of classification of images using CNNs.

The BDT analysis makes use of different kinematic features between signal and background events. The image classification-based analysis makes use of different topological features between signal and background. The addition of the CNN classification score as a BDT input variable allows the BDT to learn about kinematic features and topological features at the same time. When including the CNN classification score as one of the BDT variables, this is referred to as the (BDT+CNN) “combined analysis”. The combined analysis scheme is shown in Fig. 1.

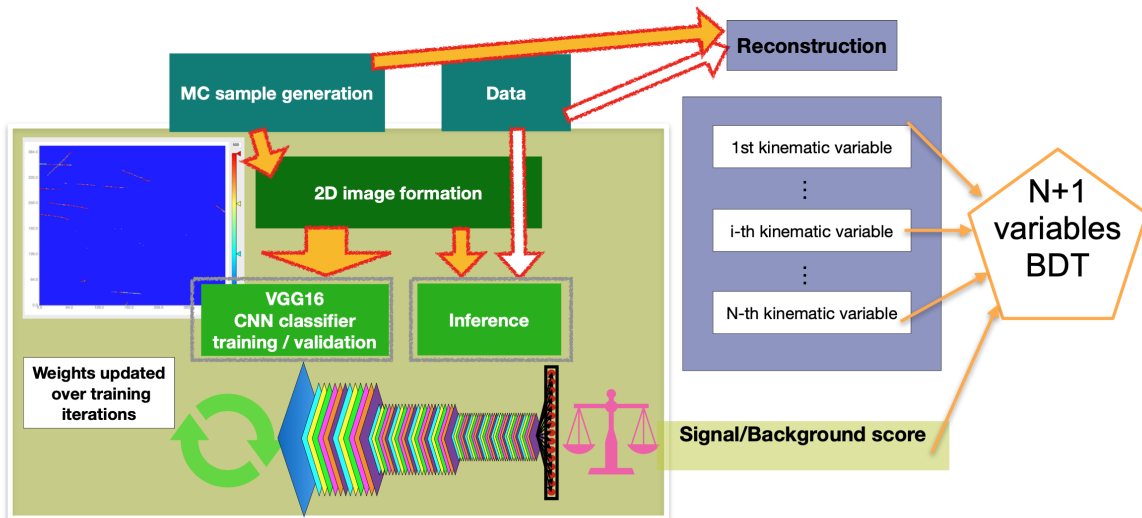


**Figure 1:** Analysis flow diagram using the (CNN+BDT) combined analysis.

Alternatively, a traditional BDT-only analysis or CNN-only analysis is possible. In the former case, the BDT is trained and optimized without the CNN score as one of the input parameters; in the latter, the CNN score is the sole classifier of signal and background events used in the event selection. In this note, we compare results from both of these to the combined analysis.

All three MicroBooNE analyses (combined, BDT-only, and CNN-only), are trained using Monte Carlo simulations. The BDT-only and the CNN-only methods are tested on a small set of data recorded with an unbiased, random trigger during MicroBooNE’s Run 1. The total Run 1 data correspond to an exposure of approx. 1400 seconds; the data used for comparisons shown in

this note correspond to an exposure of 0.82 seconds and 7.34 seconds for CNN-only and BDT-only, respectively.

The CNN training makes use of MicroBooNE signal and background Monte Carlo (MC) events. The CNN input images are constructed from collection plane wire waveforms, after hit reconstruction; each of the 3200 collection wire waveforms spans over 3.2 milliseconds of integrated readout time, digitized at 2MHz. Each of these images therefore corresponds to a  $6400 \times 3200$  pixel image, but is then down-sampled to  $400 \times 400$  before network training. Example signal and background input images (serving as “event displays”) after down-sampling are shown in Fig. 2.

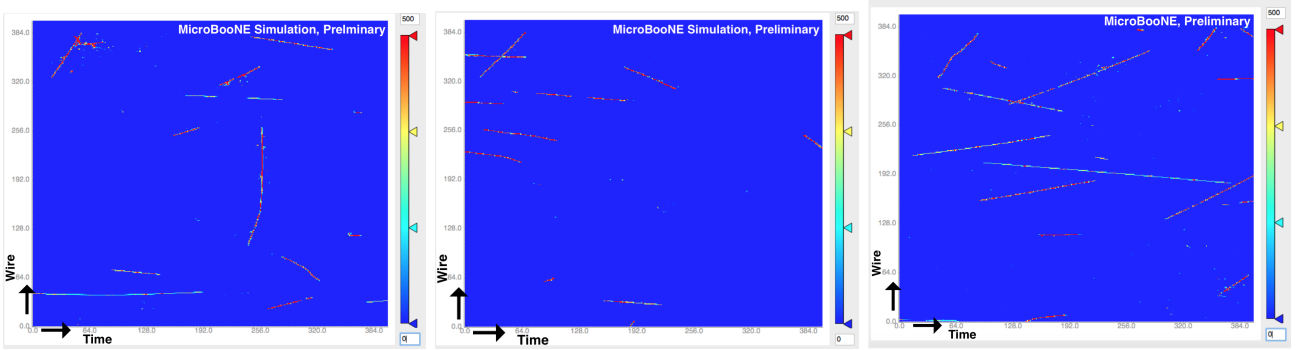


**Figure 2:** Left: Signal event display showing the  $n - \bar{n}$  signal process, with the signature shown on the top left corner, overlaid with cosmic MC, generated using MicroBooNE GENIE  $n - \bar{n}$  generation and CORSIKA[12] simulation, respectively. Middle: cosmic MC event display using MicroBooNE CORSIKA simulation only. Right: Example MicroBooNE off-beam data event (expected to be cosmic dominated). Collection plane only information is shown.

The BDT inputs use Pandora event reconstruction information, for the same MicroBooNE simulation. Pandora reconstructed “slice”(candidate neutrino interaction) selection is used to select candidate non-cosmic events, and properties of the tracks and showers associated with the selected slice are used for BDT inputs. Figure 3 shows distributions of some example BDT input variables, while the full list of BDT input variables is provided below:

- Highest (candidate interaction) slice score
- Total track energy
- Total shower energy
- Number of tracks within slice
- Leading-energy track energy
- Subleading-energy track energy
- Leading-energy shower energy
- Subleading-energy shower energy
- Leading-energy track vertex x-position
- Leading-energy track vertex y-position
- Leading-energy track vertex z-position

In the case of the combined analysis, the CNN classification score is added to the above list, and the BDT is retrained.

The following section provides preliminary results using CNN-only, BDT-only, and combined analyses.

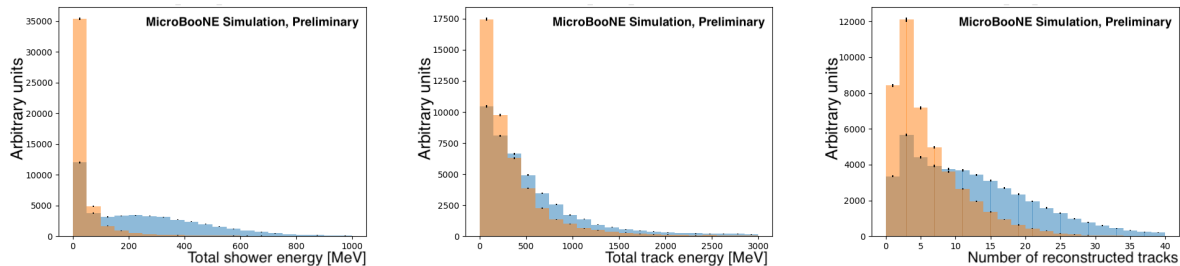


**Figure 3:** Examples of BDT input variables for cosmic MC (shown as orange histograms) and  $n - \bar{n}$  signal (shown as blue histograms). Left: total shower energy, in MeV. Middle: total track energy, in MeV. Right: track multiplicity. Each histogram is arbitrarily normalized.

### 3 Preliminary Results

#### 3.1 CNN-only analysis

The CNN image-based classification shows promising results in separating signal and background MC events. The CNN score distributions for signal MC and background MC events are shown in Fig. 4. Efficiency and background rejection performance for the CNN-only method is shown in Tab. 2 and Fig. 10.

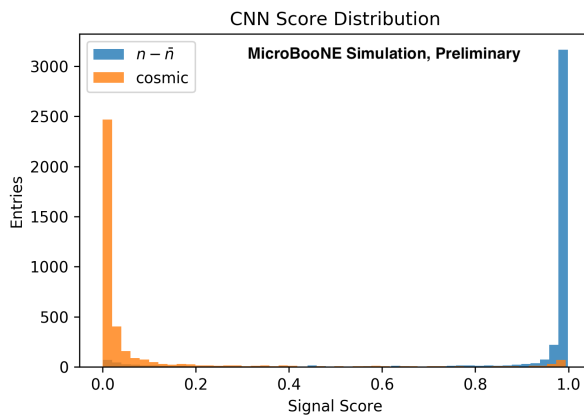


**Figure 4:** CNN classification score distributions for  $n - \bar{n}$  and cosmic background MC. A score of 1 indicates an  $n - \bar{n}$ -like event; a score of 0 indicates a cosmic-like event.

The trained network can be tested using a small subset ( $< 0.1\%$ ) of available Run 1 MicroBooNE off-beam data, corresponding to 0.82 seconds of exposure. This is shown in Fig. 5, where it is evident that the CNN score distribution of off-beam data is not consistent with that of background MC. This discrepancy in CNN response between cosmogenic MC and off-beam data is currently understood to be due to imperfect modeling of the cosmic flux and/or detector response<sup>1</sup>, and illustrates the challenge in applying MC-only-trained deep learning selections for physics data analysis. Since detector response effectively acts as a combination of “filters” on recorded data, one possible method to relieve this issue is adopting another CNN as part of the analysis, whose sole task is to explicitly target learning the “image stylistic” differences between MC-generated images and data images (see, e.g. [13]). The exploration of this method is on-going, for inclusion in the final analysis.

<sup>1</sup>Note that other MicroBooNE analyses currently make use of data overlays to emulate cosmogenic backgrounds and better approximate detector effects such as electronics noise.

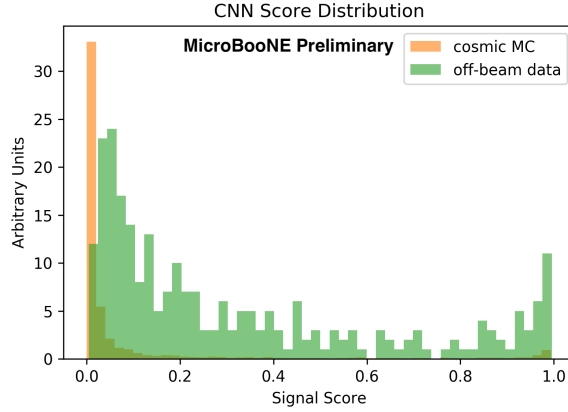


**Figure 5:** Shape-only comparison of CNN classification score distributions for MicroBooNE off-beam data (shown as green histogram, and expected to be cosmic-dominated) and cosmic background MC (shown as orange histogram).

### 3.2 BDT-only analysis

Figure 6 shows the BDT classification performance when trained using only reconstructed kinematics variables for the signal and background MC events. Efficiency and background rejection performance for the BDT-only method is shown in Tab. 2 and Fig. 10.

The BDT response is also tested using MicroBooNE off-beam data corresponding to 7.34 seconds of exposure, as shown in Fig. 7. The BDT score distribution for the off-beam data, like the CNN score distribution, also shows a different shape from the cosmic MC, having peaks on both edges of the distribution. This discrepancy, as in the case of the one for CNN response, is understood to be due to imperfect modeling of the cosmic flux and/or detector response<sup>1</sup>.

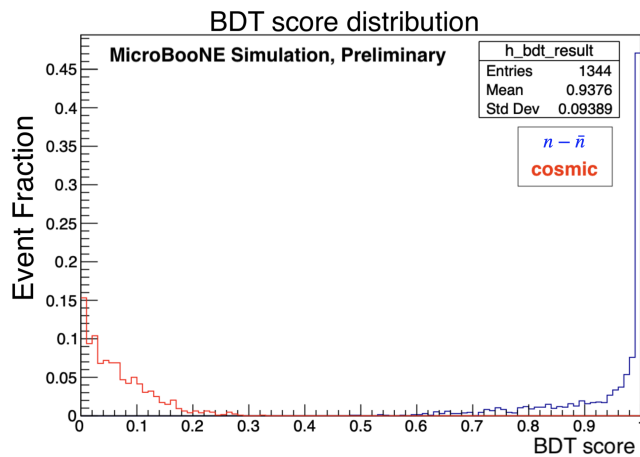


**Figure 6:** BDT score distributions for MC cosmic background (shown as red histogram) and  $n - \bar{n}$  signal (shown as blue histogram).

Event displays of off-beam events with low BDT scores are shown in Fig. 8, while event displays of off-beam events with high BDT scores are shown in Fig. 9. When tens of event displays events were examined visually, the events with high BDT scores were found to contain more TPC activity than the events with low BDT scores, on average.

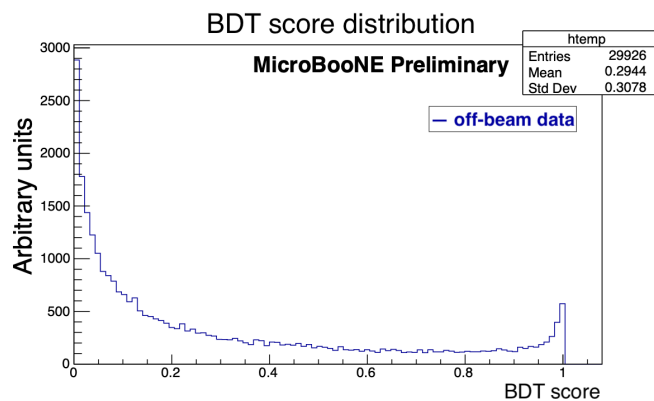


**Figure 7:** Right: BDT score distribution for MicroBooNE off-beam data (expected to be cosmic-dominated).

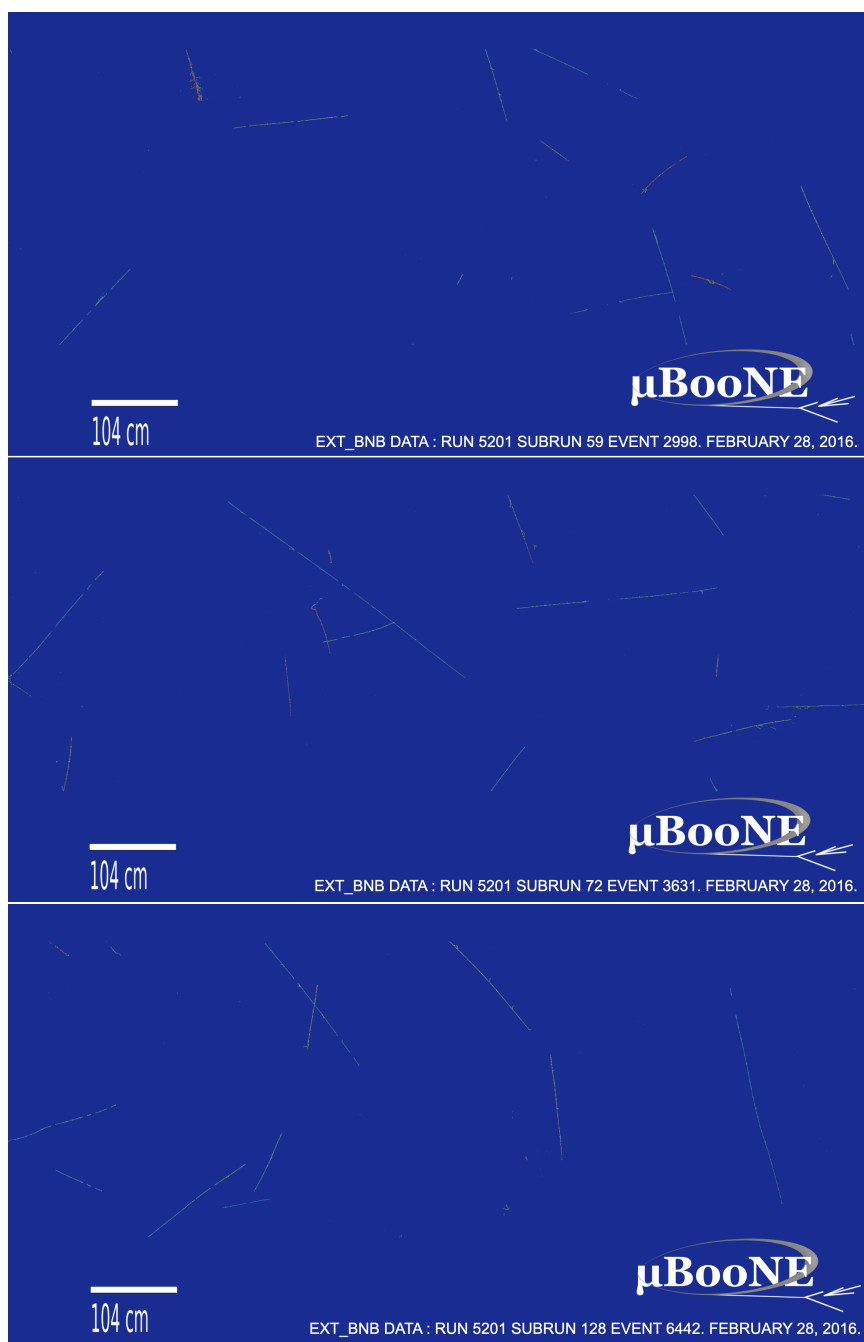


**Figure 8:** Collection plane event displays from MicroBooNE Gallery event display for low-scoring data events with the BDT-only analysis. BDT scores for top, middle, and bottom correspond to 0.0043, 0.0078, and 0.0027.

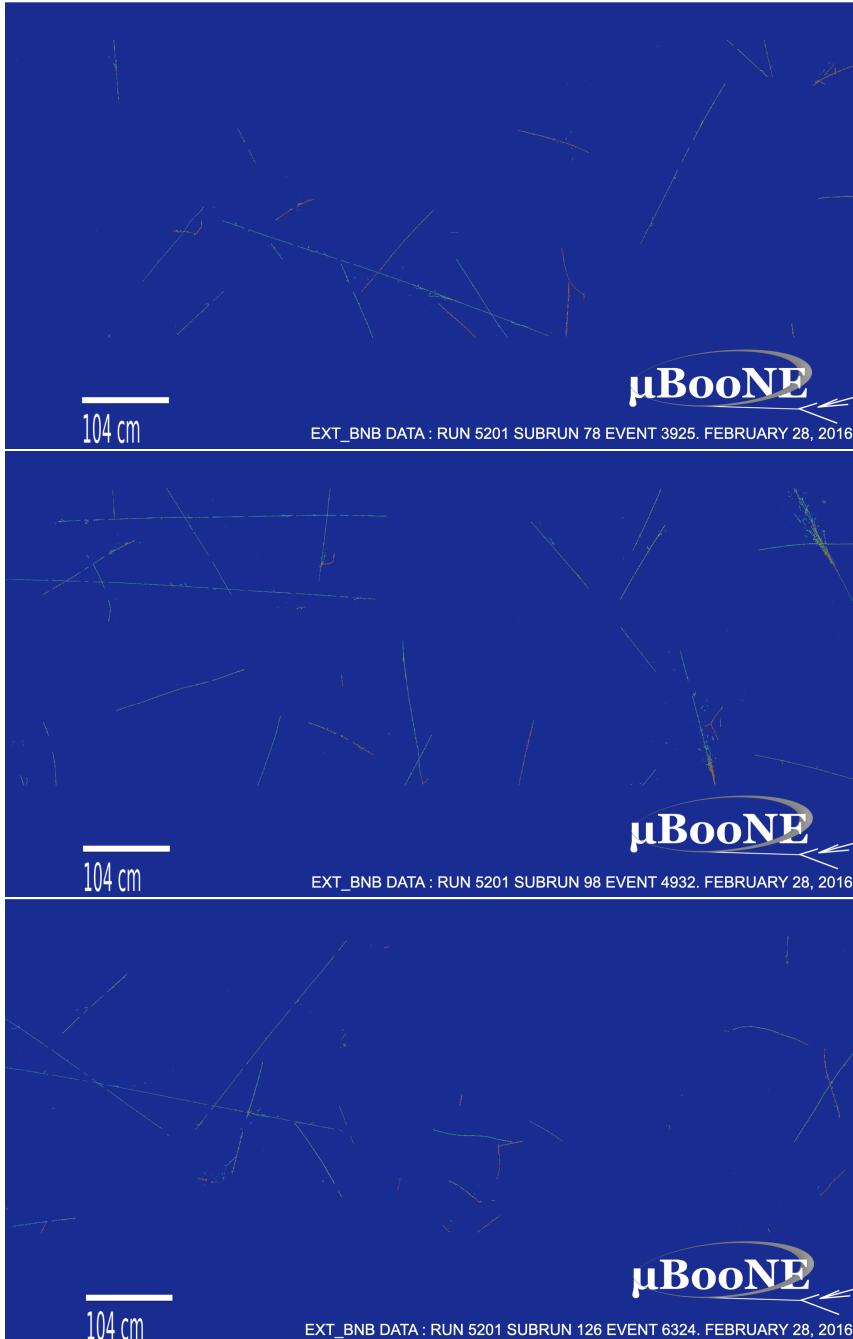


**Figure 9:** Collection plane event displays from MicroBooNE Gallery event display for high-scoring data events with the BDT-only analysis. BDT scores for top, middle, and bottom correspond to 0.968, 0.957, and 0.961.

### 3.3 Combined analysis

Preliminary classification performance using the (BDT+CNN) combined analysis is shown in Tab. 2, and compared to the performance of the BDT-only and CNN-only methods. Figure 10 shows the curves for background rejection rate vs. signal selection efficiency, where the former is defined as 1 minus background selection efficiency, for each method. The CNN-only method performs better than BDT-only. The BDT+CNN combined method shows similar performance as the CNN-only case.

The curve for the combined selection can be used to optimize sensitivity to a search for neutron-antineutron oscillation. Here, we show examples of background and signal predictions expected for an exposure of  $\sim 1400$  seconds allowed by off-beam triggers during the Run 1 of MicroBooNE.

Background rejection rate	BDT signal eff.	CNN signal eff.	BDT+CNN signal eff.
0.990	0.437	0.736	0.712
0.950	0.623	0.905	0.907
0.900	0.689	0.938	0.944
0.800	0.764	0.966	0.968
0.700	0.811	0.979	0.979
0.600	0.853	0.986	0.985
0.500	0.888	0.991	0.989

**Table 2:** Signal selection efficiencies using BDT-only (second column), CNN-only (third column), and BDT+CNN combined (fourth column) selections for a given background rejection rate (first column).

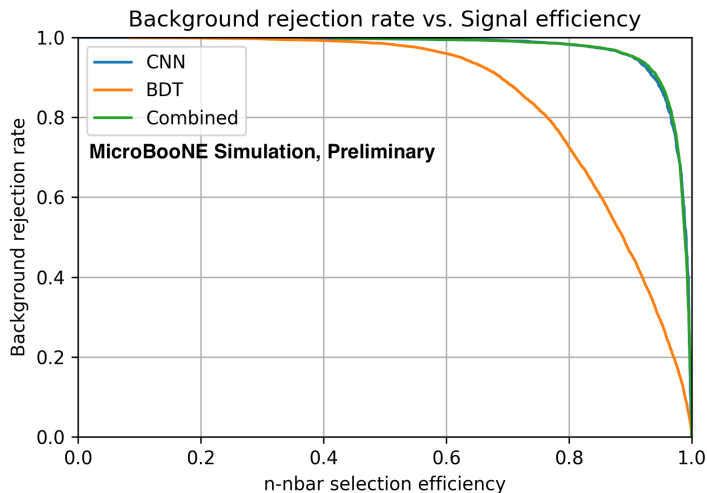


**Figure 10:** Background rejection rate versus  $n - \bar{n}$  signal efficiency achieved with the BDT-only (orange), CNN-only (blue), and BDT+CNN combined (green) analyses.

This exposure was calculated assuming 3.2 ms of off-beam trigger duration and 430,000 triggered events of the collected MicroBooNE Run 1 off-beam data. The cuts used for the BDT+CNN combined method have not been optimized to yield maximal sensitivity; instead, an example cut of BDT+CNN combined score at 0.996 is used, corresponding to a background rejection rate of 99% and signal selection efficiency of 71.5%. The resulting background and signal predictions are shown as a stacked histogram with statistical errors in Fig. 11 as a function of BDT+CNN combined BDT score; in Fig. 12 as a function of CNN score; in Fig. 13 as a function of total reconstructed energy.

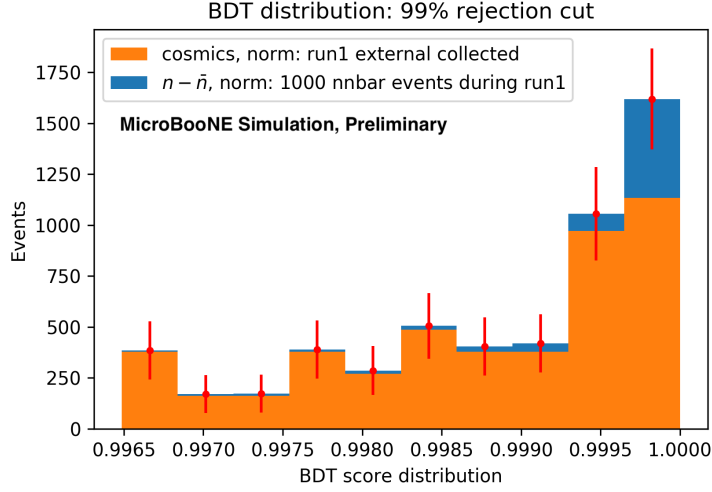


**Figure 11:** Combined score distribution for the (unoptimized) BDT+CNN combined selection, where the combined score cut is placed at a value that gives 99% rejection of the background cosmics. The background is absolutely normalized to the exposure of the off-beam data collected in MicroBooNE during the Run 1 period. The  $n - \bar{n}$  signal is normalized to an arbitrary normalization of 1000  $n - \bar{n}$  signal events in the MicroBooNE TPC during Run 1, which corresponds to  $\tau_{n-\bar{n}} = 1.27 \times 10^{24}$  years. This corresponds to  $150 \times 10^6$  times the current Super-K limit measured in  $H_2O$ , and it uses a nuclear suppression factor of  $0.517 \times 10^{23} s^{-1}$ .

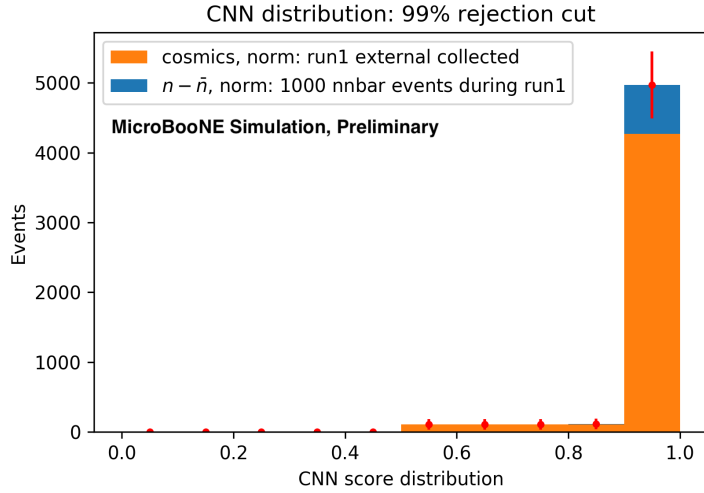


**Figure 12:** CNN score distribution for the (unoptimized) BDT+CNN combined selection, where the combined score cut is placed at a value that gives 99% rejection of the background cosmics. The background is normalized to the off-beam data collected in MicroBooNE during the Run 1 period. The  $n - \bar{n}$  signal is normalized to an arbitrary normalization of 1000  $n - \bar{n}$  signal events in the MicroBooNE TPC during Run 1, which corresponds to  $\tau_{n-\bar{n}} = 1.27 \times 10^{24}$  years. This corresponds to  $150 \times 10^6$  times the current Super-K limit measured in  $H_2O$ , and it uses a nuclear suppression factor of  $0.517 \times 10^{23} s^{-1}$ .

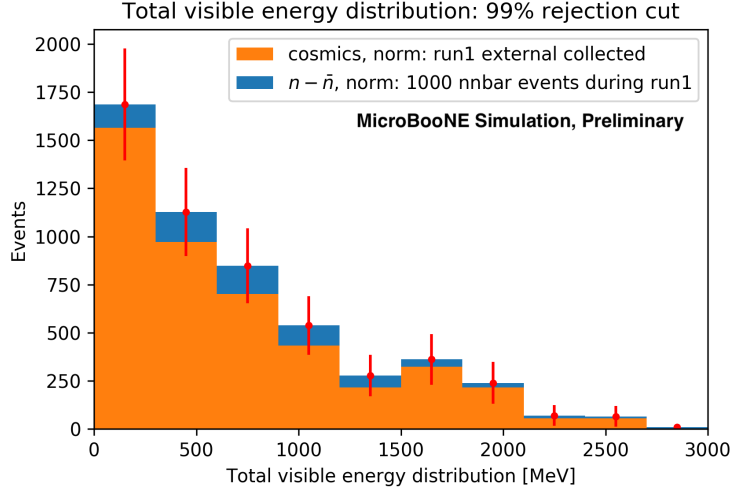


**Figure 13:** Collected energy distribution from reconstructed showers and tracks, for the (unoptimized) BDT+CNN combined selection, where the combined score cut is placed at a value that gives 99% rejection of the background cosmics. The background is normalized to the off-beam data collected in MicroBooNE during the Run 1 period. The  $n - \bar{n}$  signal is normalized to an arbitrary normalization of 1000  $n - \bar{n}$  signal events in the MicroBooNE TPC during Run 1, which corresponds to  $\tau_{n-\bar{n}} = 1.27 \times 10^{24}$  years. This corresponds to  $150 \times 10^6$  times the current Super-K limit measured in  $H_2O$ , and it uses a nuclear suppression factor of  $0.517 \times 10^{23} s^{-1}$ .

An example (unoptimized) sensitivity projection can be provided by placing the combined BDT+CNN score cut at 0.9998. The sensitivity of the  $n - \bar{n}$  lifetime can be determined for a given exposure ( $E$  in (neutron-years)), given the efficiency of selecting signal events ( $\epsilon$ ), and the background rate ( $b$ ), along with their corresponding uncertainties. Equation 1 shows the probability distribution of  $n - \bar{n}$  oscillation lifetime for a given observed number of events ( $n$ ), using Bayesian assumption where  $P(E)$ ,  $P(\epsilon)$ , and  $P(b)$  are Gaussian priors with the uncertainties of  $E$ ,  $\epsilon$ , and  $b$ .

$$P(\Gamma|n) = A \int \int \int \frac{e^{-(\Gamma\epsilon E+b)}(\Gamma\epsilon E+b)^n}{n!} P(\Gamma)P(E)P(\epsilon)P(b)dEd\epsilon db, \quad (1)$$

The 90% C.L. value for the  $n - \bar{n}$  oscillation lifetime can be found by evaluating the value of  $\Gamma_{0.9}$  that covers 90% of the total integral domain in the integral Eq. 1:

$$90\% = \frac{\int_{\Gamma=0}^{\Gamma_{0.9}} P(\Gamma|n)d\Gamma}{\int_{\Gamma=0}^{\infty} P(\Gamma|n)d\Gamma}. \quad (2)$$

When  $\Gamma_{0.9}$  in Eq.2 is found, the corresponding  $n - \bar{n}$  lifetime is given by:

$$T_{n-\bar{n}} = \frac{1}{\Gamma_{0.9}}. \quad (3)$$

The systematic uncertainties of  $E$ ,  $\epsilon$ , and  $b$  are set to be 3%, 15%, and 15%, in order to evaluate the preliminary limit, as an example. These uncertainties will be reassessed after careful systematic considerations on the signal efficiency and background efficiency of the final selection. The projected sensitivity with the unoptimized combined BDT+CNN score cut at 0.9998 and the above uncertainty assumptions would correspond to a limit of  $1.81 \times 10^{25}$  years at 90% C.L. for an exposure of  $1.18 \times 10^{27}$  neutron-years. This exposure corresponds to the entirety of Run 1 off-beam data collected in MicroBooNE. Combined score cut optimization, as well as an increase in exposure by incorporating additional data from Runs 2-5 of MicroBooNE is expected to improve the sensitivity.

## 4 Conclusions

An analysis that makes use of traditional reconstruction and deep learning based image analysis techniques has been developed to perform the first LArTPC-based search for argon-bound neutron-antineutron oscillation. The analysis is being validated on a small sample of MicroBooNE data. Although MicroBooNE is not projected to yield competitive limits to this process, because of its small size and on-surface location, this analysis serves as an important first step toward a high-sensitivity search for this process with the future DUNE detector.

The MicroBooNE analysis is ongoing, targeting further improvements in data-MC agreement from new techniques developed for image analysis, and an improved assessment of systematic uncertainties, in particular from intranuclear interaction modeling of signal, cosmic background modeling, and detector response.

# References

- [1] K.S. Babu and R.N. Mohapatra. Observable neutron anti-neutron oscillations in seesaw models of neutrino mass. *Phys. Lett. B*, 518:269–275, 2001.
- [2] Stephan J. Huber and Qaisar Shafi. Neutrino oscillations and rare processes in models with a small extra dimension. *Phys. Lett. B*, 512:365–372, 2001.
- [3] M. Baldo-Ceolin et al. A new experimental limit on neutron-antineutron oscillations. *Zeitschrift für Physik C Particles and Fields*, 63(3):409–416, 1994.
- [4] Joshua L. Barrow, Elena S. Golubeva, Eduard Paryev, and Jean-Marc Richard. Progress and simulations for intranuclear neutron-antineutron transformations in  $^{40}_{18}\text{Ar}$ . *Phys. Rev. D*, 101:036008, Feb 2020.
- [5] Costas Andreopoulos. Genie physics users manual. Genie Collaboration, 2019.
- [6] Jeremy E.T. Hewes. *Searches for Bound Neutron-Antineutron Oscillation in Liquid Argon Time Projection Chambers*. PhD thesis, Manchester U., 2017.
- [7] Babak Abi et al. Deep Underground Neutrino Experiment (DUNE), Far Detector Technical Design Report, Volume II DUNE Physics. 2 2020.
- [8] Abe, K. and others. Neutron-antineutron oscillation search at super-kamiokande. Neutrino 2020, June 22 to July 2, 2020.
- [9] R. Acciarri et al. Convolutional neural networks applied to neutrino events in a liquid argon time projection chamber. *Journal of Instrumentation*, 12(03):P03011–P03011, mar 2017.
- [10] C. Adams et al. Deep neural network for pixel-level electromagnetic particle identification in the microboone liquid argon time projection chamber. *Phys. Rev. D*, 99:092001, May 2019.
- [11] R. Acciarri et al. The pandora multi-algorithm approach to automated pattern recognition of cosmic-ray muon and neutrino events in the microboone detector. *The European Physical Journal C*, 78(1), Jan 2018.
- [12] D. Heck, J. Knapp, J. N. Capdevielle, G. Schatz, and T. Thouw. *CORSIKA: a Monte Carlo code to simulate extensive air showers*. 1998.
- [13] Jun-Yan Zhu, Taesung Park, Phillip Isola, and Alexei A Efros. Unpaired image-to-image translation using cycle-consistent adversarial networks. In *Computer Vision (ICCV), 2017 IEEE International Conference on*, 2017.